PCCP

Cite this: *Phys. Chem. Chem. Phys.*, 2012, **14**, 9336–9342

www.rsc.org/pccp

PAPER

Oxidative dehydrogenation of cyclohexene on size selected subnanometer cobalt clusters: improved catalytic performance *via* evolution of cluster-assembled nanostructures

Sungsik Lee,[a] Marcel Di Vece,[b] Byeongdu Lee,[a] Sönke Seifert,[a] Randall E. Winans[a] and Stefan Vajda*[bcd]

Received 16th January 2012, Accepted 23rd February 2012
DOI: 10.1039/c2cp40162b

The catalytic activity of oxide-supported metal nanoclusters strongly depends on their size and support. In this study, the origin of morphology transformation and chemical state changes during the oxidative dehydrogenation of cyclohexene was investigated in terms of metal-support interactions. Model catalyst systems were prepared by deposition of size selected subnanometer $Co_{27\pm4}$ clusters on various metal oxide supports (Al_2O_3, ZnO and TiO_2 and MgO). The oxidation state and reactivity of the supported cobalt clusters were investigated by temperature programmed reaction (TPRx) and *in situ* grazing incidence X-ray absorption (GIXAS) during oxidative dehydrogenation of cyclohexene, while the sintering resistance monitored with grazing incidence small angle X-ray scattering (GISAXS). The activity and selectivity of cobalt clusters shows strong dependence on the support. GIXAS reveals that metal-support interaction plays a key role in the reaction. The most pronounced support effect is observed for MgO, where during the course of the reaction in its activity, composition and size dynamically evolving nanoassembly is formed from subnanometer cobalt clusters.

Introduction

Cyclic hydrocarbon conversion to benzene is important in petroleum refining and reforming processes.[1] To develop a new catalyst for cyclohexane conversion, it would be greatly helpful to understand support and size effects in the conversion of the cyclohexene intermediate since the rate determining step in the dehydrogenation of cyclohexane to benzene is the dehydrogenation of the cyclohexene intermediate. This step requires specific orientation of the adsorbed cyclohexene relative to the catalyst surface, thus a catalytic particle with optimal size and morphology.[2,3] Therefore, dehydrogenation of cyclohexene has been used for key kinetic and structure-function studies for cyclohexane dehydrogenation.[4–6] A reaction mechanism is proposed where the σ-adsorption is followed by a stepwise elimination of H_2 from cyclohexane to cyclohexene and cyclohexadiene intermediates, and the π–σ shift of the adsorbed cyclohexene is identified as a rate determining step.[7] Adsorption and reaction studies carried out using cyclohexane, cyclohexene, 1,3-cyclohexadiene, and benzene on the Pt(111) surface also suggest that cyclohexane conversion to cyclohexene and dehydrogenation of 1,3-cyclohexadiene to benzene proceeds rapidly to completion.[2]

Because of its high activity and selectivity, most of the studies have concentrated on Pt[8–10] and its alloys[5,8,11] as catalysts, however, non-precious metal catalysts have drawn more attention recently.[1,4,11–13] Cobalt is one of the promising candidates for oxidative dehydrogenation (ODH) of cyclohexane. In addition, cobalt is known as a good oxidation catalyst such as in the transformation of cyclohexane to KA oil (cyclohexanone–cyclohexanol mixture).[14–16] Only very few studies have been reported on cobalt based cyclohexene dehydrogenation catalysis.[17] In addition, oxidative dehydrogenations[1,13,17,18] by cobalt catalyst can overcome a thermodynamic limitation of dehydrogenation of cyclohexane (endothermic, ΔH = 49.3 kcal mol^{-1})[12] and coking issues which cause deactivation of catalyst.

A logical pathway to the development of such non-precious metal catalyst is the tailoring of the catalyst size control and of support properties.[4,15,19] To develop in size and composition, well defined tailored catalyst, it is essential to combine sophisticated high-fidelity materials fabrication with atomic precision and *in situ* characterization tools to understand the behavior and nature of the catalyst under realistic reaction conditions. Thus, the activity of catalysts needs to be followed along with the evolution of catalyst's

[a] *X-ray Science Division, Argonne National Laboratory, 9700 South Cass Avenue, Argonne, IL 60439, USA*
[b] *Department of Chemical and Environmental Engineering, Yale University, 9 Hillhouse Avenue, New Haven, CT 06520, USA*
[c] *Materials Science Division, Argonne National Laboratory, 9700 South Cass Avenue, Argonne, IL 60439, USA*
[d] *Center for Nanoscale Materials, Argonne National Laboratory, 9700 South Cass Avenue, Argonne, IL 60439, USA. E-mail: vajda@anl.gov*

size/shape, its sintering-resistance and chemical state during the course of the reaction.

Here we report catalytic cyclohexene conversion to benzene, which is the rate determining step in cyclohexane to benzene conversion reaction, in the oxidative dehydrogenation on supported, size selected cobalt clusters. The correlation between catalytic properties and support-metal interactions is discussed using *in situ* grazing incidence X-ray absorption spectroscopy (GIXAS) and grazing incidence small angle X-ray scattering (GISAXS) data collected on these systems, coupled with temperature-programmed reaction (TPRx). The high surface sensitivity of grazing incidence techniques, including GISAXS and GIXAS enables the study the chemical state and morphology of metal nanoparticles deposited on flat substrate with less than one tenth of monolayer coverage. GISAXS has been proven to be a very powerful tool to study morphological transformations of nanoparticles under a reactive gas environment under atmospheric pressure.[19–25] Recently published series of reports show successful employments of various combinations of the GISAXS, GIXAS and TPRx techniques.[19,21–23,26]

1. Experimental

For catalyst support materials, 3 ML thick amorphous MgO, Al_2O_3, ZnO, and TiO_2 films were prepared by atomic layer deposition (ALD) on the top of a naturally oxidized silicon wafers (SiO_2/Si(100))[13,19,21,23] using a custom viscous flow ALD reactor. The size-selected cobalt cluster catalysts were prepared by depositing a narrow size-distribution of cobalt clusters generated in a laser vaporization cluster source. The size-selected cluster deposition method was described in detail elsewhere.[19,21,23,25,27,28] In brief, a molecular beam of cobalt clusters was prepared by laser vaporization of a cobalt target with helium as carrier gas. Then, the beam was guided through an ion optics and quadrupole assembly, and the mass-selected, positively charged clusters soft-landed (<1 eV/atom) on the support.[25] The amount of deposited cobalt metal was determined by real-time monitoring of the deposition flux.[25] The surface coverage at the deposition spots was 0.1 ML equivalent of Co metal; the corresponding Co loading, 11.6 ng was kept identical in each sample. The uncertainty in the determination of the metal loading was 10% or better.[25,26]

The X-ray experiments were performed using a unique setup developed at the Sector 12-ID-C at the Advanced Photon Source of the Argonne National Laboratory.[29] The schematic of the combined TPRx/GISAXS/GIXAS experiment is shown in Fig. 1. GISAXS was performed with 8 keV X-rays in a home built reaction cell with an internal volume of 25 cm^3.[29] The cluster sample was placed on the top of the ceramic heater center in the cell. The cell was sealed with Kapton windows and mounted on a computer controlled goniometer. A 1024 × 1024 pixel two-dimensional CCD detector (MarCCD) was used for recording the GISAXS images from the sample. GISAXS data were collected as a function of reaction temperature and time. The collected data were processed and analyzed by FitGISAXS package.[30] GIXAS data were collected by a 4-element fluorescence detector (Vortex 4 element SDD) mounted perpendicular to the X-ray beam

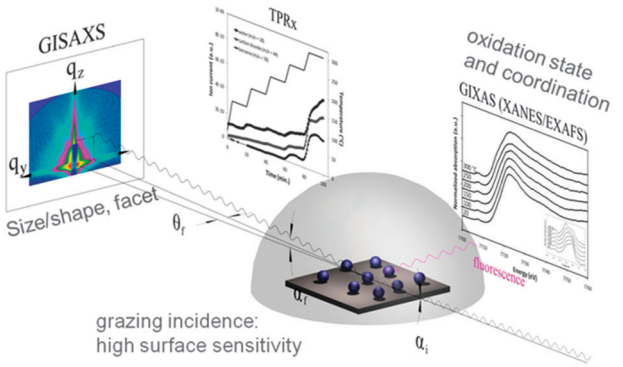

Fig. 1 Schematic of system setup for combined *in situ* GISAXS, GIXAS and TPRx experiment.

and parallel to the sample surface as a function of reaction temperature and time. The collected data were analyzed using the IFEFFIT interactive software package (with ATHENA and ARTEMIS graphical interfaces).[31]

During the GISAXS/GIXAS characterization, simultaneous reactivity measurements were also conducted. The gas reactants used were 4000 ppm cyclohexene in helium and 99.9% oxygen (AirGas), and the ratio for cyclohexene and O_2 was kept at 1 : 10 by preparing the mixture in a remotely controlled gas-mixing unit consisting of calibrated mass flow controllers (Brooks model SLA5850). The reaction cell was operated in a 30 cm^3 min^{-1} continuous flow mode at 800 torr. The products were analyzed using a differentially pumped mass-spectrometer (Pfeiffer Vacuum Prisma Plus QMS 220 M2). The reaction temperature was controlled by heating the sample placed on the top of the ceramic heater (Momentive Performance Materials Inc.) with a K-type thermocouple attached to the edge of the heater surface and a temperature controller (Lakeshore model 340) for precision temperature control (< ± 0.5 °C). To achieve thermal equilibrium between the heater and sample during the application of a temperature ramp, a low heating rate (<10 °C min^{-1}.) was used between temperature steps. 15 min were spent at each temperature, to provide sufficient time for the collection of GISAXS and GIXAS data.

For the on-line analysis of the gas mixture which was extracted from the reaction cell during the course of the reaction, the mass spectrometer was operated in continuous mass scanning mode (1 scan/min.) which allows for a simultaneous monitoring of the ion current corresponding to a mass range of up to 100 amu for the reactants and all possible reaction products. The fragment patterns from the standard gases were also compared with the NIST mass spectra of benzene, carbon dioxide and water as well as other possible reaction products. To quantify the reactants and products, the sensitivity factors of the mass spectrometer for individual molecules were calculated using calibrated gas mixtures (certified analytical grade mixed gas, Air Gas Inc.). The uncertainty was estimated to be ~2% of the ion current. The TPRx data collected for the cluster samples were backround corrected by using TPRx background signals obtained by using a blank support (*i.e.* identical wafer without deposited clusters) with identical temperature ramp and reaction conditions as applied for the cluster samples. The calculation of the turn-over rates (TOR) was based on the

total count of deposited cobalt atoms. Taking into consideration an estimated 10% uncertainty in the determination of the number of deposited atoms, the error in determination of the turn-over rates was estimated to be about 10%.[26]

2. Results and discussion

The normalized XANES spectra (Co-K edge) of Co clusters supported on MgO and Al_2O_3 are presented in Fig. 2 as a function of reaction temperature. The Co samples are first measured in helium background at room temperature and then in cyclohexene and oxygen mixture at indicated temperatures. The XANES spectra (Co-K) of the as prepared sample and the spectra in reaction gas environment up to 200 °C are similar to each other and show a broad XAS feature. Based on comparison with bulk standards, up to 200 °C, the main part of cobalt species in the samples is present as a CoO dominant phase mixed with Co_3O_4 under applied reaction conditions. A sudden change occurs at 250 °C in the Co/MgO sample, which includes forming a sharper peak at 7727 eV and distinct two shoulder feature at lower energy. The changes are more pronounced at 300 °C, and no further change are observed within the 45 min time interval at this temperature, which indicates this form is stable at the temperature. The well developed new features are clearly observed in Co/MgO sample starting at 250 °C, while the Al_2O_3 supported cobalt shows only a broadening in white line feature and slight change in near the edge region, which further develops with increasing temperature. The change in Co/MgO sample indicates transformation to a higher oxidation state, Co_3O_4, or surface alloy like $Co_xMg_{1-x}O$ with the MgO support.[32–34] Presumably, at high temperature cobalt and MgO form a mixed oxide which drives oxidation state and structural changes. MgO is known to be a non-reducible oxide, and our concurrent study shows that ZnO, TiO_2, and Al_2O_3 supported cobalt catalysts do not show similar change in cobalt oxidation state under identical reaction conditions. A subtle change occurs during the cooling ramp, the lower energy shoulder feature diminished, and the cobalt feature

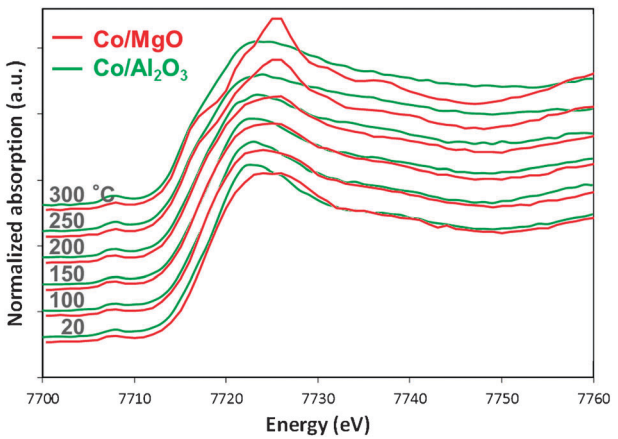

Fig. 2 Co K-edge XANES spectra of Co/MgO (red) and Co/Al_2O_3 (green) from bottom to up in the order of reaction temperatures, 20, 100, 150, 200, 250 and 300 °C, respectively. Cyclohexene (0.39%) and oxygen (3.90%) in He at total pressure of 800 torr.

returns close to Co_3O_4, which indicates that $Co_xMg_{1-x}O$ formed at 300 °C may be stable only at high temperature. The Co-K edge feature of $Co_xMg_{1-x}O$ has been reported to be very sensitive to the stoichiometry in $Co_xMg_{1-x}O$.[32] It is well known that Co–Mg–O solid solution can be formed at relatively low temperatures (<100 °C)[34,35,41] and that high concentration of weakly chemisorbed oxygen species result in Co–Mg–O solid solution as a good catalyst for hydrolysis of glycerol,[34] N_2O catalytic decomposition,[35,41] CO_2 reforming of CH_4[33] and ethanol steam reforming,[42] although the reducibility of cobalt oxides is greatly decreased in the Co_3O_4/MgO precursor.[35] The temperature-dependent change in XANES feature of the Co/MgO cluster sample can be well correlated with the reported spectra of $Co_xMg_{1-x}O$ which change with Mg content.[32] The spectrum of the Co/MgO sample at 250 °C closely resembles the spectrum of $Co_xMg_{1-x}O$ with Co fraction of $x = 0.67$, while the spectrum of clusters at 300 °C indicates a dramatic increase in the Mg content, with the fraction of Co as low as $x = 0.10$. The differences between the spectral features of Co/MgO and $Co_xMg_{1-x}O$ at energies above ~7.73 keV presumably arise from a Co_3O_4 fraction present in the cluster sample, however an (additional) contribution from subnanometer effects cannot be entirely excluded at this point. Quantitative determination of the fraction of each mixed oxide state is greatly complicated since CoO, Co_3O_4 and Co, as well as with a temperature evolving distribution of $Co_xMg_{1-x}O$ compositions can coexist, and the bulk reference spectra do not necessary represent subnanometer clusters due to: (a) intrinsic electronic structure difference between subnanometer clusters and bulk state and (b) strong interaction between small clusters and support oxides.

In situ GISAXS shows a clear difference between the Co sample evolution depending of the support. GISAXS data collected on cobalt clusters supported on Al_2O_3 (Fig. 3a), TiO_2 and ZnO do not reveal any changes in particle size under reaction conditions, thus providing evidence about the sintering-resistance of the cobalt clusters during two hours of reaction. Fig. 3 shows temperature dependent line cut (horizontal) profiles and typical 2D-GISAXS image of Co/MgO sample. The 2-D linecut data has been fitted to particle size and distribution as shown in Fig. 3c. At room temperature, GISAXS represent dominant substrate scattering with a little contribution from cobalt nanoparticles, which indicates that the clusters are in subnanometer size range, as-prepared. At the applied surface coverage and photon energy used a quantitative analysis of particles smaller than 1 nm is rather difficult, because of the roughness of metal oxide supports prepared by ALD method, which have a ≤1 nm of surface roughness. Moreover, the roughness of the MgO surface is expected to change because during the reaction a fraction of the surface Mg(O) dissolves in the supported clusters, forming Co–Mg–O particles. Since such changes in the support roughness are not possible to deconvolute from the total scattering, the interpretation of the data is limited to particle sizes larger than 1nm. A slight change in the GISAXS pattern is noticeable in the small q range (~1 nm^{-1}) at 250 °C, followed by the most significant change observed at 300 °C, which indicates the formation of nanostructure with very sharp size distribution. For the GISAXS data fitting, supported island model with log normal distribution

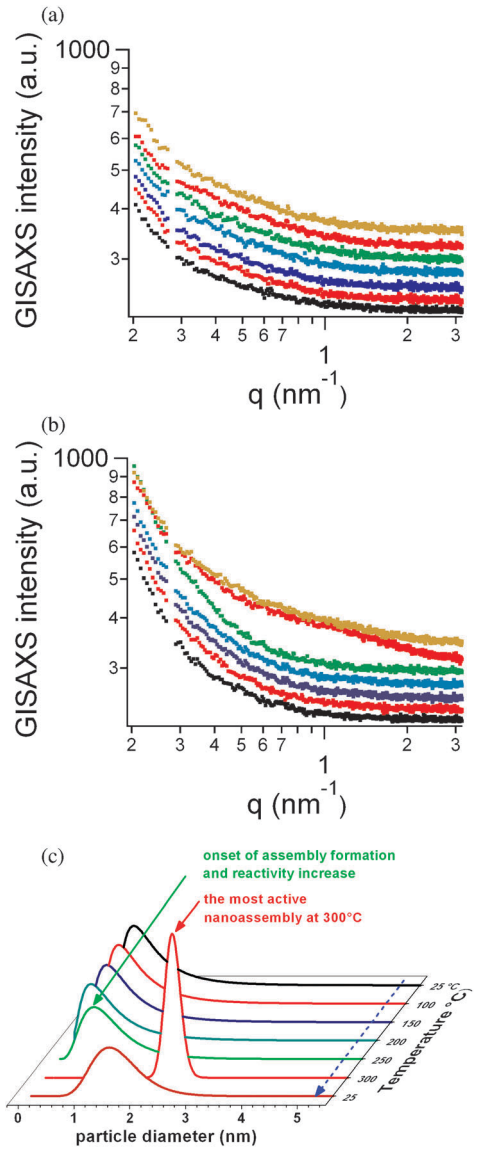

Fig. 3 GISAXS intensity (horizontal line cut) change during the heating cycle, from the bottom 20, 100, 150, 200, 250, 300 and 20 °C (after reaction) respectively for (a) alumina-supported and (b) magnesia-supported cobalt clusters; the spectra are offset for clarity. (c) evolution of particle/nanoassembly size distribution of the magnesia-supported clusters during the reaction. Cyclohexene (0.39%) and oxygen (3.90%) in He at total pressure of 800 torr.

has been used with FitGISAXS program.[30] At 300 °C, the nanoclusters transform into ~2.5 nm × 1.6 nm (diameter × height) nanostructures with a narrow size distribution. More interesting features appeared when the sample was cooled down to room temperature. The average particle size shrank to ~1.8 nm with a ~2 nm broad size distribution. This sequence of changes cannot be simply interpreted by thermal sintering because of reversible change during the cooling cycle and unique feature development only on Co/MgO system. Since MgO is a non-reducible support, there is no strong electronic effect between cobalt and MgO, which could facilitate chemical transformation from CoO to other form of oxides. Presumably, well dispersed subnanometer cobalt clusters can be transformed to Co–Mg–O solid solution rather easily in oxidation environment at high temperature,[33–35] and the preformed metastable Co–Mg–O cluster solid solution can be in good part reversibly transformed to CoO*x*–MgO system at low temperature. Also, we note that the increased final ~1.8 nm lateral diameter of the clusters after reaction could arise from the combination of altered shape of the building cluster blocks, as well as from larger clusters that retained a fraction of Mg(O) from the solid Co–Mg–O solution formed at 300 °C.

As discussed in the Introduction, the dehydrogenation of cyclohexene is structure sensitive and it is essential to provide well accessible two or three fold binding sites for cyclohexene to transform to benzene.[4–6] Unlike the other metal oxides supported clusters, Co/MgO has a highly dynamically evolving structure and forms 2–3 nm size particles at 300 °C during the reaction, which presumably adapts to provide the needed binding sites for cyclohexene and other reaction intermediates during dehydrogenation to benzene. The size effect on cyclohexene dehydrogenation on Pt nanoparticles has been reported with various particle sizes. It shows that the rate of dehydrogenation of cyclohexene to benzene decreases monotonically over the particle size range from 1 to 9 nm.[4] It clearly shows that the size is critical for the reaction rate while the optimum size and structure of the active site could be strongly dependent on the system.

Fig. 4 (a) and (b) show the TPRx profile of oxidative dehydrogenation of cyclohexene on Co/MgO and Co/Al_2O_3 systems, respectively. Major reaction products are CO_2, water and benzene.

There are no KA oil related products observed during the reaction in any of the subnanometer cobalt cluster based catalysts. Most of side products are CO_2 and water from the total oxidation of cyclohexene. At 300 °C, the cyclohexene signal decreases at 300 °C by ~18% for the Co/MgO system and by ~10% for the Co/Al_2O_3, Co/ZnO and Co/TiO_2 systems from the initial signal level at room temperature. In addition to main reaction products (benzene, CO_2 and water), a trace amount of cyclohexadiene is also observed at ~250 °C, but disappears at higher temperatures at which benzene formation becomes more dominant. Presumably, electronically localized nature of small size cobalt cluster suppresses formation of radical intermediates for oxidation of cyclohexene. Also, the relatively stable adsorption complex which is formed between cyclohexene and cobalt catalyst may be less favorable for radical formation than one from cyclohexane and cobalt.

With the *in situ* GISAXS data, it is possible to unambiguously distinguish between support and size effects in the systems studied. Up to temperatures of 200 °C, the clusters retain their subnanometer size on all four supports, thus their catalytic performance can be discussed as function of the support. The support effects for the Co/ZnO, Co/TiO_2, and Co/Al_2O_3 systems can be also compared up to 300 °C. However, in the case of the Co/MgO system, above 200 °C the performance is assigned to nanometer size structures assembled from subnanometer Co cluster building blocks, moreover with evolving complex composition/oxidation state as indicated by *in situ* GIXAS.

The Co/Al_2O_3, Co/TiO_2 and Co/ZnO systems show similar activity (Fig. 4c) and selectivity (Fig. 4d), with Co/ZnO possessing the highest activity and selectivity towards benzene production in the entire temperature region among the Co/Al_2O_3, Co/TiO_2

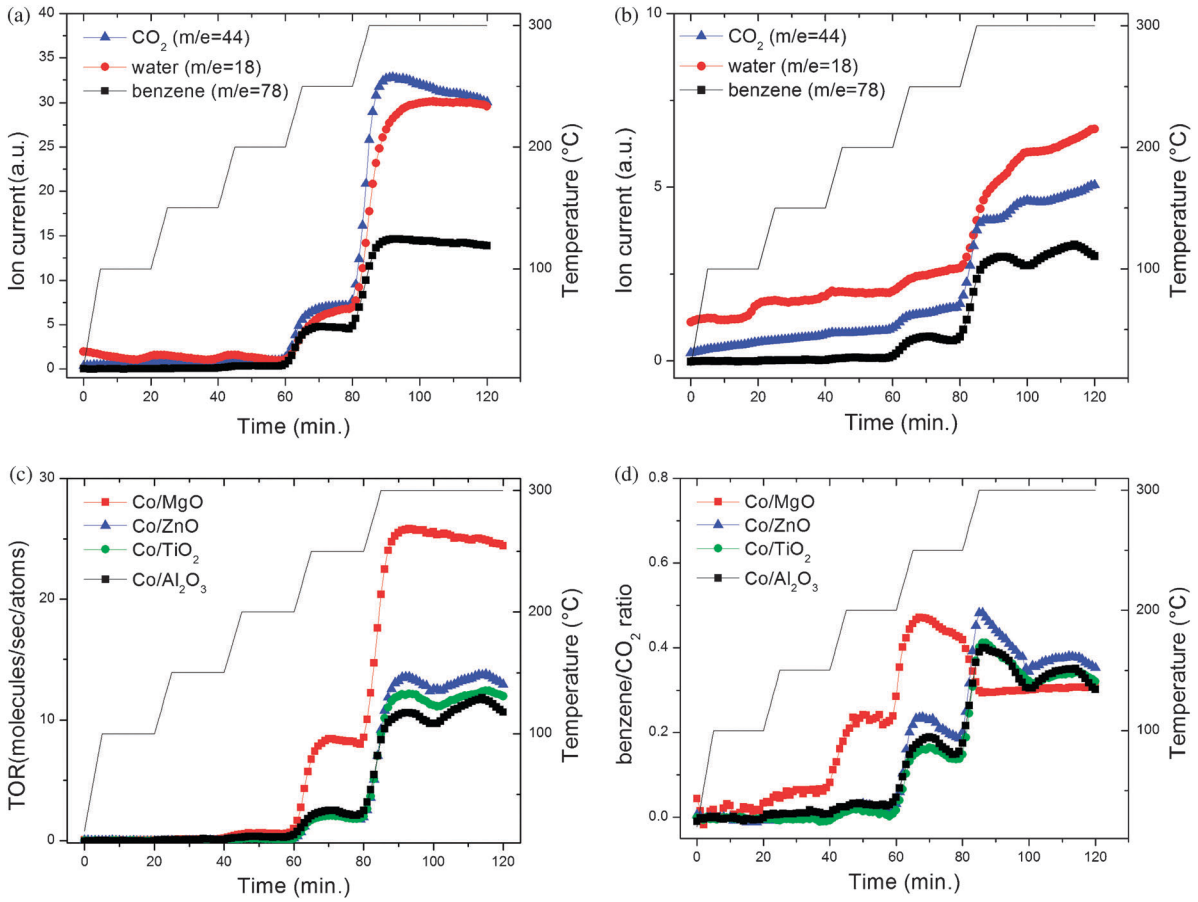

Fig. 4 (a) Background-corrected TPRx profile of benzene, water and carbon dioxide evolution on Co/MgO sample during the oxidative dehydrogenation of cyclohexene. (b) Background-corrected TPRx profile of benzene, water and carbon dioxide evolution on Co/Al_2O_3 sample (an offset was applied to the curves for better clarity). (c) Turnover rate of benzene formation on Co/MgO, Co/ZnO, Co/TiO_2, and Co/Al_2O_3. The straight line shows the temperature profile ramping from 20 to 300 °C, stepwise. Evolution of benzene is shown as turnover rate per cobalt atom. Cyclohexene (0.39%) and oxygen (3.90%) in He at total pressure of 800 torr. (d) selectivity plot (carbon weighted) between benzene and CO_2 on Co/MgO, Co/ZnO, Co/TiO_2, and Co/Al_2O_3 during the temperature ramping as shown in the straight line. (Fig. 4b adapted with permission from ref. 29).

and Co/ZnO trio. However, in the subnm size region (*i.e.* up to 200 °C), the Co/MgO system clearly outperforms all the other systems (Fig. 4c and d). Especially, at low temperature benzene selectivity of MgO at 150 and 200 °C is about order of magnitude higher than the ones from Co/Al_2O_3, Co/TiO_2 and Co/ZnO. This indicates that the Co/MgO cluster has an intrinsic difference in electronic structure even before to form a Co-Mg-O solid solution.

In extended time of reaction at 300 °C the Co/Al_2O_3, Co/ZnO and Co/TiO_2 systems show oscillatory behavior in their activity (Fig. 4c). Since during the time window of the measurement at 300 °C only two cycles could be observed, based on the limited data we can only hypothesize that the observed oscillations strongly resemble oscillations in reactivity induced by cyclic adsorption–desorption of reactants, products or intermediates during the oxidation of CO oxidation[36–38] or benzaldehyde.[39] Unfortunately, the current XANES setup is not optimized for quick XAS to track the changes in chemical state change of the catalyst on this timescale. Even more interestingly, the formation of CO_2 and benzene seems competing with each other during the oscillatory isothermal reaction, with a lowered fraction of benzene produced at points of lowered activity (see activity and selectivity at 100 and 120 min in Fig. 4c and d, respectively).

Per cobalt atom temperature-dependent turnover rates of benzene formation on Co/MgO, Co/Al_2O_3, Co/TiO_2 and Co/ZnO systems reveal significantly increased activity at 250 °C for all four systems, however the by a factor of ~2–3 higher activity of the Co/MgO correlates with the change of the oxidation state/composition of the catalytic particles (*cf.* XANES in Fig. 2) and the assembly of subnanometer clusters into a nanostructure (see GISAXS, Fig. 3c). At 250 °C, the ~1.5 nm assembly formed in the Co/MgO system outperforms Co/Al_2O_3, Co/TiO_2 and Co/ZnO in both activity and selectivity. However at 300 °C, though the ~2.5 nm structure of the Co/MgO system still exhibits the highest activity, the Co/Al_2O_3, Co/ZnO and Co/TiO_2 systems have somewhat higher selectivity towards benzene formation. Onset of product formation on subnanometer cobalt clusters is observed at 150 °C, which demonstrates the capability of sub-nm (oxidized) cobalt clusters to activate O_2 at low temperatures.

Oxidative dehydrogenation studies on cyclohexene are scarce.[1,40] Recently published results based on TiO_2 supported Au, Pd and Au–Pd catalyst show high activity at relatively low temperatures; 99% benzene selectivity and 100% conversion at 150 °C.[1] On the contrary, under the same conditions over Co-ZSM5, the cyclohexane conversion becomes significant only at temperatures above 430 °C and increases to 45% by increasing the temperature to 610 °C.[1] The main products at low conversion are CO_x whereas at higher temperature benzene becomes the most important product.[18] For comparison, vanadia based catalyst has been reported for ODH of cyclohexane with relatively high reaction temperature (>400 °C).[13,18] These examples on cyclohexane dehydrogenation (since cyclohexene dehydrogenation the rate limiting step) demonstrate that (bulkier) cobalt and vanadia based ODH catalysts have a considerably higher light off temperature than their subnanometer size cobalt counterparts.

3. Conclusions

The presented results show that oxide-supported catalysts made of subnanometer cobalt clusters have a light up temperature around 150 °C and maintain high reactivity up to 300 °C in the oxidative dehydrogenation of cyclohexene, while their activity and selectivity towards benzene formation strongly depends on the support used and on the size and oxidation state/composition of the active particles. The low light off temperature and observed turnover rates can make such materials attractive alternatives to precious metal based dehydrogenation catalysts, but also for other oxidative processes.

The most interesting finding behind the high activity of MgO supported catalyst is the dynamic formation of a cluster-based nanoassembly composed of a solid oxide $Co_xMg_{1-x}O$ and Co_3O_4 like mixture during the reaction. These highly dynamic nanostructures seem to adapt their size and morphology to offer optimal active sites for the reaction.

Summing it up, the presented study demonstrats that the performance of subnanometer cobalt catalysts can be tuned by the size and composition of the catalyst as well as support used, and that *in situ* GISAXS/GIXAS are instrumental at the identification of the size and nature of the working catalysts under realistic reaction conditions.

Acknowledgements

The authors thank Drs Jeffrey W. Elam and Joseph A. Libera for providing the metal oxide–coated substrates. This material is based upon work supported by the US Department of Energy, BES Materials Sciences and Scientific User Facilities under Contract DE-AC02-06CH11357 with UChicago Argonne, LLC, operator of Argonne National Laboratory. MDV and SV acknowledge the support provided by the U.S. Air Force Office of Scientific Research under AFOSR MURI grant FA9550-08-0309. This paper is a contribution to the special issue of Phys. Chem. Chem. Phys., honouring, at the occasion of his 65th birthday, the life work of Ludger Wöste, whose pioneering cluster studies were and will remain inspirational for decades to come. One of the authors (SV) had the unique opportunity and great pleasure working with Ludger in Berlin. Lieber Ludger, your enthusiasm and optimism shall never fade. Happy Birthday!

References

1 N. F. Dummer, S. Bawaked, J. Hayward, R. Jenkins and G. J. Hutchings, *Catal. Today*, 2010, **154**, 2–6.
2 J. L. Gland, K. Baron and G. A. Somorjai, *J. Catal.*, 1975, **36**, 305–312.
3 B. E. Koel, D. A. Blank and E. A. Carter, *J. Mol. Catal. A: Chem.*, 1998, **131**, 39–53.
4 R. M. Rioux, B. B. Hsu, M. E. Grass, H. Song and G. A. Somorjai, *Catal. Lett.*, 2008, **126**, 10–19.
5 Z. Paal, A. Wootsch, D. Teschner, K. Lazar, I. E. Sajo, N. Gyorffy, G. Weinberg, A. Knop-Gericke and R. Schlogl, *Appl. Catal., A*, 2011, **391**, 377–385.
6 R. B. Borade, B. Zhang and A. Clearfield, *Catal. Lett.*, 1997, **45**, 233–235.
7 M. E. Ruiz-Vizcaya, O. Novaro, J. M. Ferreira and R. Gómez, *J. Catal.*, 1978, **51**, 108–114.
8 L. I. Ali, A.-G. A. Ali, S. M. Aboul-Fotouh and A. K. Aboul-Gheit, *Appl. Catal., A*, 1999, **177**, 99–110.
9 K. R. McCrea and G. A. Somorjai, *J. Mol. Catal. A: Chem.*, 2000, **163**, 43–53.
10 B. E. Nieuwenhuys, D. I. Hagen, G. Rovida and G. A. Somorjai, *Surf. Sci.*, 1976, **59**, 155–176.
11 S. L. Lu, W. W. Lonergan, J. P. Bosco, S. R. Wang, Y. X. Zhu, Y. C. Xie and J. G. Chen, *J. Catal.*, 2008, **259**, 260–268.
12 J. Escobar, J. Reyes, T. Viveros and M. C. Barrera, *Ind. Eng. Chem. Res.*, 2006, **45**, 5693–5700.
13 H. Feng, J. W. Elam, J. A. Libera, M. J. Pellin and P. C. Stair, *J. Catal.*, 2010, **269**, 421–431.
14 J. H. Tong, L. L. Bo, Z. Li, Z. Q. Lei and C. G. Xia, *J. Mol. Catal. A: Chem.*, 2009, **307**, 58–63.
15 Y. M. Liu, H. Tsunoyama, T. Akita, S. H. Xie and T. Tsukuda, *ACS Catal.*, 2011, **1**, 2–6.
16 I. Hermans, J. Peeters and P. A. Jacobs, *J. Phys. Chem. A*, 2008, **112**, 1747–1753.
17 E. P. De Garcia, M. R. De Goldwasser, C. F. Parra and O. Leal, *Appl. Catal.*, 1989, **50**, 55–63.
18 M. Panizza, C. Resini, G. Busca, E. Fernández López and V. Sánchez Escribano, *Catal. Lett.*, 2003, **89**, 199–205.
19 S. Lee, Luis M. Molina, María J. López, Julio A. Alonso, B. Hammer, B. Lee, S. Seifert, Randall E. Winans, Jeffrey W. Elam, Michael J. Pellin and S. Vajda, *Angew. Chem., Int. Ed.*, 2009, **48**, 1467–1471.
20 B. Lee, S. Seifert, S. J. Riley, G. Tikhonov, N. A. Tomczyk, S. Vajda and R. E. Winans, *J. Chem. Phys.*, 2005, **123**, 74701.
21 S. Lee, B. Lee, F. Mehmood, S. Seifert, J. A. Libera, J. W. Elam, J. Greeley, P. Zapol, L. A. Curtiss, M. J. Pellin, P. C. Stair, R. E. Winans and S. Vajda, *J. Phys. Chem. C*, 2010, **114**, 10342–10348.
22 J. A. Balmer, O. O. Mykhaylyk, S. P. Armes, J. P. A. Fairclough, A. J. Ryan, J. Gummel, M. W. Murray, K. A. Murray and N. S. J. Wiliams, *J. Am. Chem. Soc.*, 2011, **133**, 826–837.
23 Y. Lei, F. Mehmood, S. Lee, J. Greeley, B. Lee, S. Seifert, R. E. Winans, J. W. Elam, R. J. Meyer, P. C. Redfern, D. Teschner, R. Schlogl, M. J. Pellin, L. A. Curtiss and S. Vajda, *Science*, 2010, **328**, 224–228.
24 R. E. Winans, S. Vajda, G. E. Ballentine, J. W. Elam, B. Lee, M. J. Pellin, S. Seifert, G. Y. Tikhonov and N. A. Tomczyk, *Top. Catal.*, 2006, **39**, 145–149.
25 S. Vajda, R. E. Winans, J. W. Elam, B. Lee, M. J. Pellin, S. Seifert, G. Y. Tikhonov and N. A. Tomczyk, *Top. Catal.*, 2006, **39**, 161–166.
26 L. M. Molina, S. Lee, K. Sell, G. Barcaro, A. Fortunelli, B. Lee, S. Seifert, R. E. Winans, J. W. Elam, M. J. Pellin, I. Barke, V. v. Oeynhausen, Y. Lei, R. J. Meyer, J. A. Alonso, A. Fraile-Rodríguez, A. Kleibert, S. Giorgio, C. R. Henry, K.-H. Meiwes-Broer and S. Vajda, *Catal. Today*, 2011, **160**, 116–130.
27 W. Deng, S. Lee, S. Vajda, J. A. Libera, J. W. Elam and C. L. Marshall, *Appl. Catal., A*, 2011, **393**, 29–35.
28 S. Vajda, M. J. Pellin, J. P. Greeley, C. L. Marshall, L. A. Curtiss, G. A. Ballentine, J. W. Elam, S. Catillon-Mucherie, P. C. Redfern, F. Mehmood and P. Zapol, *Nat. Mater.*, 2009, **8**, 213–216.

29 S. Lee, B. Lee, S. Seifert, S. Vajda and R. E. Winans, *Nucl. Instrum. Methods Phys. Res., Sect. A*, 2011, **649**, 200–203.
30 D. Babonneau, *J. Appl. Crystallogr.*, 2010, **43**, 929–936.
31 B. Ravel and M. Newville, *J. Synchrotron Radiat.*, 2005, **12**, 537–541.
32 A. Kuzmin, N. Mironova and J. Purans, *J. Phys.: Condens. Matter*, 1997, **9**, 5277–5286.
33 H. Y. Wang and E. Ruckenstein, *Appl. Catal., A*, 2001, **209**, 207–215.
34 X. H. Guo, Y. Li, R. J. Shi, Q. Y. Liu, E. S. Zhan and W. J. Shen, *Appl. Catal., A*, 2009, **371**, 108–113.
35 N. Russo, D. Fino, G. Saracco and V. Specchia, *Catal. Today*, 2007, **119**, 228–232.
36 B. Kimmerle, A. Baiker and J. D. Grunwaldt, *Phys. Chem. Chem. Phys.*, 2010, **12**, 2288–2291.
37 E. S. Kurkina and N. L. Semendyaeva, *Surf. Sci.*, 2004, **558**, 122–134.
38 Y. Gong, Z. Hou and H. Xin, *J. Phys. Chem. B*, 2004, **108**, 17796–17799.
39 M. G. Roelofs, E. Wasserman and J. H. Jensen, *J. Am. Chem. Soc.*, 1987, **109**, 4207–4217.
40 E. C. Alyea and M. A. Keane, *J. Catal.*, 1996, **164**, 28–35.
41 U. Chellam, Z. P. Xu and H. C. Zeng, *Chem. Mater.*, 2000, **12**, 650–658.
42 S. Tuti and F. Pepe, *Catal. Lett.*, 2008, **122**, 196–203.

